Journal of Circuits, Systems, and Computers
Vol. 26, No. 4 (2017) 1750055 (20 pages)

DOI: 10.1142/S0218126617500554

An Enhanced Design of Multi-Band RF Band Pass Filter Based on Tunable High-Q Active Inductor for Nano-Satellite Applications*

Aymen Ben Hammadi[†,¶], Mongia Mhiri[†,‖], Fayrouz Haddad[‡,**], Sehmi Saad[†,††] and Kamel Besbes[§,‡‡]

[†]*Microelectronics & Instrumentation Laboratory, Faculty of Sciences of Monastir, University of Monastir, Boulevard of Environment, Monastir 5019, Tunisia*

[‡]*Aix Marseille Université, CNRS, Université de Toulon, IM2NP UMR 7334, 13397 Marseille, France*

[§]*Centre for Research on Microelectronics & Nanotechnology Sousse Technology Park, 4000 Sousse, Tunisia*

[¶]*aymen.benhammadi@fsm.rnu.tn*
[‖]*mongia.mhiri@fsm.rnu.tn*
[**]*fayrouz.haddad@im2np.fr*
[††]*sehmi.saad@fsm.rnu.tn*
[‡‡]*kamel.besbes@fsm.rnu.tn*

Received 24 May 2016
Accepted 5 September 2016
Published 19 October 2016

This paper describes the design of a novel cascode-grounded tunable active inductor and its application in an active band-pass filter (BPF) suitable for multi-band radio frequency (RF) front-end circuits. The proposed active inductor circuit uses feedback resistance to improve the equivalent inductance and the quality factor. The novelty of this work lies on the use of a few number of multi-finger transistors, which allows reducing strongly the power consumption and the silicon area. In other words, we demonstrate that the use of variable P-type Metal-Oxide-Semiconductor (PMOS) resistor and controllable current source have a good potential for wide tuning in terms of inductance value, quality factor and frequency operation. The RF BPF is realized using the proposed active inductor with suitable input and output buffer stages. The tuning of the center frequency for multi-band operation is achieved through control voltages. The designed active inductor and RF BPF have been implemented in a standard 0.13 μm Complementary Metal Oxide Semiconductor (CMOS) technology. The simulation results are compared between schematic and post-layout design for inductance value, quality factor, transmission coefficient S21 and noise. This design yields encouraging results: the inductance value can be tuned from 10.94 to 44.17 nH with an optimal quality factor around 2,581. In addition, the center frequency of the BPF can be tuned between 2 and 4.84 GHz with

*This paper was recommended by Regional Editor Piero Malcovati.
¶Corresponding author.

an average insertion loss of 10.92 ± 0.31 dB. Throughout this range, the noise figure is between 10.49 and 9.22 dB with an input referred 1 dB compression point of -0.25 dBm and IIP3 of 7.36 dBm. The filter occupies $25.43\,\mu m \times 21.56\,\mu m$ of active area without pads and consumes between 2.38 and 2.84 mW from a 1 V supplying voltage.

Keywords: Tunable active inductor; feedback resistor; high quality factor; multi-band; band-pass filter.

1. Introduction

The rapid growth of wireless communication applications, such as mobile and nano-satellite systems, has led to the development of high performance integrated transceivers capable to operate in different frequency bands.[1] In these systems, band-pass filter (BPF) is one of the most important modules and its miniaturization is a key challenge. To incorporate many desired communication bands in a single unit, filters with multi-band responses are essential for these communication systems. The compact size, low noise figure, low power consumption, wide tuning center frequencies range and better linearity are the most important requirements in the design of these components.[2,3]

In a conventional design of BPF, on-chip spiral inductors are often used as a building block due to their high linearity, simple structure and power handling capability. However, their application is limited and they have many disadvantages such as; low quality factor, large chip area and difficulty of achieving wide range of tuning ability as reported in Ref. 4.

In several approaches, these issues can be alleviated by using varactor-diodes to provide a wide tuning range. In compensation, the varactors consume large area and have less tuning range due to the limitation of the ratio between their maximum and minimum capacitance (around 30%).[4]

Concerning the current mode approach, the most versatile building block is the active filter based on active inductors that have been used in a wide range of applications since their emergence. Therefore, from Refs. 5–10, using this component allows to overcome the disadvantages of passive structure and to satisfy the required performances. In fact, active inductor, which is properly designed using only transistors, which occupies less than 10% of passive inductor's area, and it can be continuously tuned to operate over a wide frequency range. In addition, an active inductor provides a large inductance value with a high quality factor (Q) and high resonance frequency. So it has important advantages, but it has some disadvantages such as higher noise, nonlinearity and power consumption that should be taken into account in the design process. Also, among these problems, low gain and poor noise performance are critical challenging issues in BPF designs.[6] Nevertheless, our research group has chosen to work with the current-mode approach owing to its reputed advantages[11] that have been demonstrated in several works like in implementing some functions[12] and analog multipliers[13] etc. This paper explains in details

the concept of tunable high-Q active inductor and applies it to the design of a reconfigurable active BPF for application in S-band. Note that S-band is the range of frequency from 2 to 4 GHz which is a part of frequency band used by nano-satellite applications.

Using reconfigurable feedback resistance and cascode stage, an approach improves the performances of classic active inductor adopting that would ultimately enhance the quality factor. It also provides low power consumption and achieves miniaturization of the circuit compared to the traditional active inductor. Furthermore, in order to meet the needs of high tunability of the quality factor and inductance, two kinds of tuning phenomenon occur in this circuit. The first tuning is implemented at the level of feedback resistance by acting on the variation of the DC voltage of the gate-source PMOS transistor. The second tuning is achieved at the system level where current variation is performed by an external control.

Subsequently, multi-band BPF is realized by using the tunable active inductor. The extra advantages that arise from the use of the proposed circuit are the improved noise, the miniaturized size and the flexibility in modulating the center frequency of the filter. The characteristics of BPF are clearly indicating, including frequency tuning ranges, noise, linearity and power consumption. To verify the proposed concept, layout of the circuit is generated and post-layout simulation is performed.

The paper is organized as follows. Section 2 explains the concept of our active inductor and discusses its advantages versus traditional structure. Section 3 describes the proposed multi-band BPF. Schematic and post-layout simulations with discussion are covered in Sec. 4. Finally, conclusions are given in Sec. 5.

2. Tunable Active Inductor Design

2.1. *Cascode-grounded active inductor with feedback resistor*

The most common active inductor topology is the cascode-grounded active inductor as shown in Fig. 1(a). This circuit is based on gyrator topology, that contains only two current sources for the biasing and two transistors (where the drain of the first is connected to the gate of the second), generating the inductive impedance.

In order to enhance the quality factor of the active inductor, a feedback resistor R_f is connected between the transconductors g_{m1} and g_{m2} realized, respectively, by transistors M_1 and M_2. On the other hand, a transistor M_3 is employed to reduce the output conductance (g_{ds}) which enhances the inductance L and the quality factor Q as explained in Refs. 14–16. Using the small signal equivalent model of the common-grounded active inductor, shown in Fig. 1(b), the impedance and the quality factor are expressed as follows:

$$Z_{\text{in}} \approx \frac{R_{\text{eq}} + j\omega L_{\text{eq}}}{-L_{\text{eq}} C_{\text{eq}} \omega^2 + j(G_{\text{eq}} L_{\text{eq}} + R_{\text{eq}} C_{\text{eq}})\omega + G_{\text{eq}} R_{\text{eq}} + 1}\,, \tag{1}$$

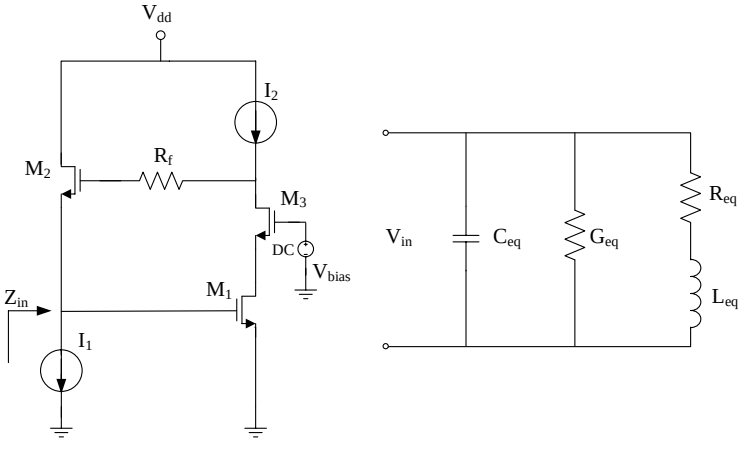

Fig. 1. (a) The cascode-grounded active inductor with resistive feedback topology and (b) its equivalent circuit.

$$Q \approx \frac{\omega L_{\text{eq}}\left(1 - \dfrac{C_{\text{eq}} R_{\text{eq}}^2}{L_{\text{eq}}} - \omega^2 C_{\text{eq}} L_{\text{eq}}\right)}{R_{\text{eq}}\left(G_{\text{eq}} R_{\text{eq}}\left(\dfrac{\omega^2 L_{\text{eq}}^2}{R_{\text{eq}}^2} + 1\right) + 1\right)} . \tag{2}$$

Analyzing the extracted linear model of inductor circuit given by Fig. 1(a), the corresponding parameters in the equivalent model of Fig. 1(b) are expressed as follows:

The equivalent capacitance as:

$$C_{\text{eq}} = C_{gs1} , \tag{3}$$

the equivalent conductance as

$$G_{\text{eq}} = \frac{R_f g_{ds3}^2 + 2 g_{ds3}}{g_{ds3} R_f + 1} , \tag{4}$$

the equivalent resistance as

$$R_{\text{eq}} = \frac{(C_{gs2}^2 g_{m3} - C_{gs2} C_{gs3} g_{m2}(G_{ds3} R_f + 1))\omega^2 + g_{ds1} g_{ds3} g_{m2}}{g_{m1} g_{m2}^2 g_{m3}} \tag{5}$$

and the equivalent inductance as:

$$L_{\text{eq}} \approx \frac{C_{gs2}^2 C_{gs3}(G_{ds3} R_f + 1)\omega^2 + g_{m2} g_{m3} C_{gs2}}{g_{m1} g_{m2}^2 g_{m3}} . \tag{6}$$

Referring to Eqs. (2) and (6), adding a feedback resistance R_f between the transistors M_1 and M_2, it will be possible to boost the active inductor quality factor and/or to improve the inductance value.[17]

2.2. *Design considerations of the proposed active inductor*

There are many proposed CMOS circuit implementations of the well-known gyrator-based inductor.[18–22] The circuit implementation in this work incorporates the required degrees of freedom to facilitate the desired tuning of both of inductance value and quality factor. A key feature is the use of feedback resistor and current sources as mechanisms to improve the tuning ranges of L and Q.

A simplified schematic of the proposed tunable active inductor is given in Fig. 2(a). It is based on using the cascode-grounded topology (Fig. 1) in order to further enhance the inductance value and the quality factor. In fact, the addition of the transistor M_3 stacks on the top of M_1, reduces the equivalent conductance g_{ds1}. Then, the equivalent resistance is decreased and the equivalent inductance is greatly increased as described in Refs. 19 and 20.

This circuit is also based on the use of an active feedback resistance M_4 added between transistors M_2 and M_3. This feedback resistance forms an additional inductive reactance of the impedance looking in to the source terminal of M_2, which can significantly increase the inductance of the cascode-grounded active inductor. Furthermore, the inductance increase results in an increased quality factor.

The current sources I_1 and I_2 are implemented using transistors (M_7, M_8) and (M_5, M_6), respectively.

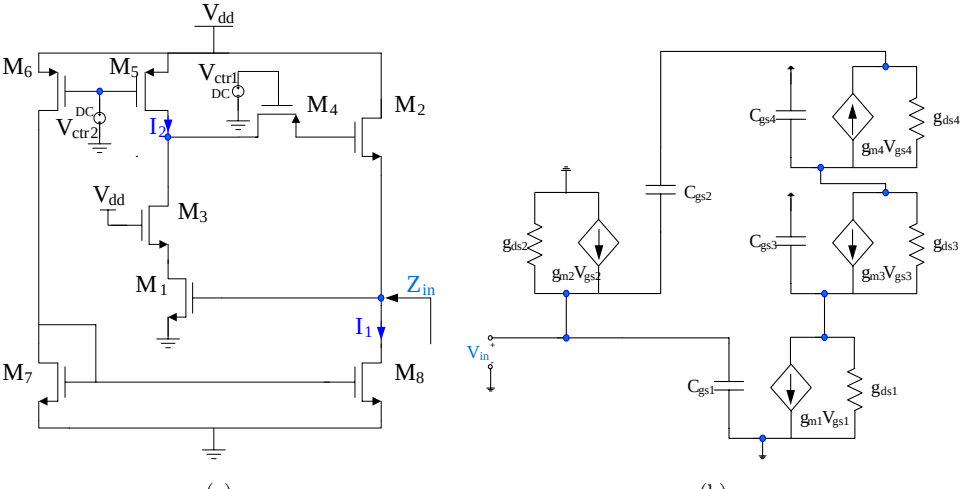

(a) (b)

Fig. 2. Proposed radio frequency (RF) CMOS tunable active inductor topology and equivalent circuit.

Assuming that the current sources are ideal, the equivalent small signal model of the proposed tunable active inductor is shown in Fig. 2(b). The equivalent inductance can be expressed as follows:

$$L_{\text{eq}} = \frac{g_{m1}g_{m2}C_{gs1} + \omega^2 C_{gs1}^2 C_{gs2}\left(\frac{g_{ds3}}{g_{ds4}} + 1\right)}{g_{m1}^2 g_{m2} g_{m3} + \omega^2 C_{gs1}^2 g_{m2} g_{m3}} . \tag{7}$$

2.3. *Tuning of the proposed active inductor*

There are many ways to vary the inductance value.[21–23] In the proposed Tunable Active Inductor (TAI) design, two tuning techniques are used to achieve this goal. The first technique, referring to Eq. (7), consists in varying the feedback resistor R_f value. In this work, this component is replaced by a PMOS transistor controlled by the voltage V_{ctr1}, which is preferred in cascode-grounded structure. In fact, PMOS transistors have low noise performance and can be placed in separate n-wells, resulting in the elimination of nonlinear body effects.[20] Thus, by varying the DC voltage, V_{ctr1} of the gate-source of the PMOS transistor, the output conductance of M_4 is changed leading to a variation of the equivalent feedback resistance. This proves the possibility to control and to reconfigure the active inductor.

The second technique to adjust the inductance is to modify the current bias in the circuit. In fact, according to Eq. (7), the inductance value and the quality factor depend on g_{m1}, g_{m2}, g_{m3} and R_f (feedback resistance) which are greatly affected by current sources I_1 and I_2. In this case, the current source I_2 have been designed based on a voltage-controlled transistor. The adjustment of the voltage control V_{ctr2} can change at the same time the currents I_1 and I_2.

The novelty of this design is that the inductance adjustment method can be ensured via tuning of the active feedback resistor together with the current sources. In comparison to the active inductor presented in Refs. 22–26, the proposed design uses a circuit topology that reduces the current consumption. This is realized by current sources instead of the PMOS load transistors.

3. BPF Design Based on Active Inductor

In order to validate its efficiency, the proposed tunable active inductor has been applied to the implementation of a second-order RF BPF as it is widely used in wireless communication systems. Its topology belongs to the class of LC resonance-based filters.[27]

In the following, we briefly discuss the proposed BPF architecture and its linear model.

3.1. *Filter structure*

There are many proposed CMOS circuit implementations of BPFs based on active inductor as cited in several works.[6,7,26,28,29] The circuit implementation used in this work incorporates the required degrees of freedom to facilitate tuning to the desired center frequency, bandwidth and center frequency gain.

Hence, based on the proposed active inductor, a second-order RF BPF implementation, useful for multi-band integrated circuit radio applications, has been designed. Its complete circuit schematic is shown in Fig. 3.

The filter is composed by three RF stages including the previous proposed active inductor, input and output buffers. The common source NMOS transistor M_{in} is used as the input buffer stage for input matching, it is capable to convert the input voltage V_{in} to a current that is applied to the active inductor. The source-follower output buffer stage for output matching is composed of NMOS transistor M_{out} and the controlled gate transistor M_9 which replaces the current source I_B. This buffer is included to prevent the load from severely affecting the filter's frequencies and Q. Moreover, the input and output buffers are capable of driving off-chip 50Ω loads over a wide RF frequency range.

The voltages V_{ctr1} and V_{ctr2} are used for the bias voltages of the transistors M_4–M_6, respectively. However, the V_{bias} voltage is applied to the transistor gate M_9, used as current source.

By varying the DC voltages, V_{ctr1} and V_{ctr2}, the inductance value changes automatically varying the center frequency of the filter.

All transistors have the minimum channel length of 0.13 μm. Transistor M_4 is set to work in linear region and all other transistors are set to work in the saturation region. The sizes of these transistors are optimized to reach a high performance of the

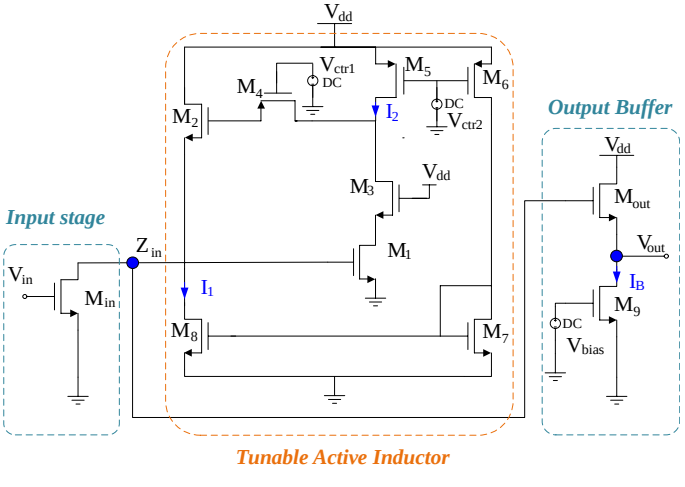

Fig. 3. Proposed RF multi-band BPF.

Table 1. Design parameters of RF BPF.

Transistor	Number of fingers	W/L (μm)
M_{in}, M_{out}	5	60/0.13
M_1	2	18/0.13
M_2	2	20/0.13
M_3	2	22/0.13
M_4, M_6, M_8	1	5/0.13
M_5	1	8/0.13
M_7	1	2/0.13

filter regarding, high linearity, wide tuning range, low noise and low power consumption. The design parameters of the proposed active BPF are summarized in Table 1.

3.2. *Equivalent circuit of BPF*

Figure 4 shows the equivalent small signal model of the proposed single pole BPF using a second-order parallel RLC resonator corresponding to the active inductor mentioned in previous section. The latter is inserted between two matching networks that allow providing input and output adaptation to 50 Ω and in another hand, to provide for the resonator a high impedance slightly modifying its quality factor.

With reference to Fig. 4, the transfer function without the output stage can be expressed as follows:

$$\frac{V_r}{V_e} = A_0 \frac{2j\xi\dfrac{\omega}{\omega_0}}{1 + 2j\xi\dfrac{\omega}{\omega_0} - \left(\dfrac{\omega}{\omega_0}\right)^2}, \tag{8}$$

where the gain-bandwidth, the pole frequency and ξ are given by

$$A_0 = \frac{-g_m L_{eq}}{(L_{eq}G_{eq} + R_{eq}C_{eq})}, \tag{9}$$

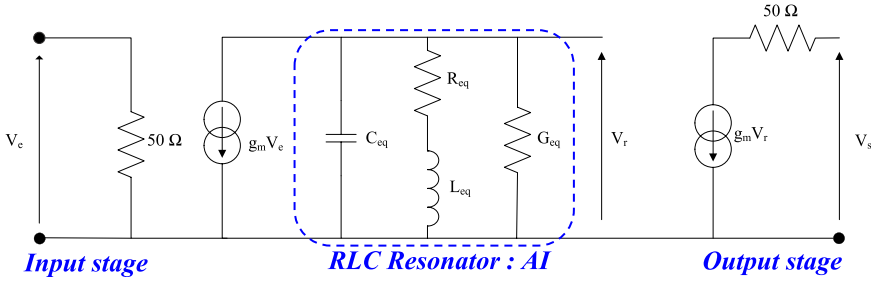

Fig. 4. Small signal equivalent circuit of the proposed second-order BPF.

$$\omega_0 = \sqrt{\frac{1 + R_{\text{eq}} G_{\text{eq}}}{L_{\text{eq}} C_{\text{eq}}}}, \tag{10}$$

$$\xi = \frac{1}{2\sqrt{1 + R_{\text{eq}} G_{\text{eq}}}} \left[G_{\text{eq}} \sqrt{\frac{L_{\text{eq}}}{C_{\text{eq}}}} + R_{\text{eq}} \sqrt{\frac{C_{\text{eq}}}{L_{\text{eq}}}} \right]. \tag{11}$$

4. Simulation and Discussion

The proposed circuits have been designed and implemented in a standard 0.13-μm CMOS technology.

Figure 5 shows the layout of the designed BPF based on active inductor which is utilized to perform post-layout simulations. Indeed, Fig. 5(a) describes the design which contains five decoupling capacitors, tow pads GSG for input and output RF signals, pad V_{dd} for voltage supply, pad gnd for ground and tow pads I/O for control voltages. However, Fig. 5(b) shows the layout of the proposed filter without pads. It contains the input stage (area dotted in yellow color), the output stage composed by two transistors (area dotted in red color) and the proposed tunable active inductor composed by eight transistors (dotted in orange color). The total area of RF filter with pads is 160 μm^2, nevertheless, the layout areas of the filter and the active inductor without pads are, respectively, 25.14 $\times$ 12.21 μm and 25.14 $\times$ 21.56 μm.

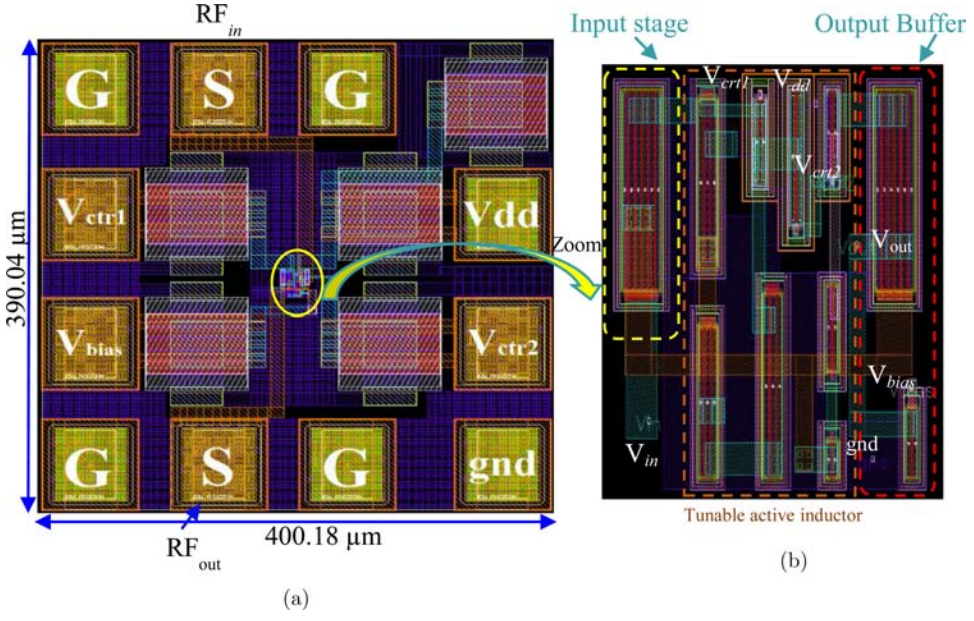

Fig. 5. Layout of multi-band RF BPF: (a) with pads, (b) without pads (color online).

Post-layout simulations have been achieved using Spectre RF simulator of Cadence®, taking into account the parasitic effects.

In this section, the TAI post-layout simulation results in terms of resonance frequency, inductance value and quality factor tuning are studied. Then, BPF post-layout simulation results in terms of resonance frequency, noise, linearity and power consumption are discussed.

4.1. *Active inductor*

The obtained frequency responses of the proposed tunable active inductor are shown in Fig. 6. The figure depicts a comparison between schematic and post-layout simulations using the RCC extraction mode. It is clear that the obtained post-layout results have a total matching with the schematic results.

Furthermore, when the control voltages V_{ctr1} and V_{ctr2} vary from 0.3 to 0.43 V and from 0.39 to 0.45 V, respectively, the inductance value varies from 10.94 to 44.17 nH. The operating frequency range is limited by 1.76 and 6.55 GHz. The control voltages have been calibrated in order to obtain an inductive behavior and a high quality factor in each case.

As shown in Fig. 6(b), the tunable Q is varying from 323 @ 1.15 GHz to 684 @ 4.58 GHz. A maximum quality factor of almost 2,581 is attained at 2 GHz, when V_{ctr1} and V_{ctr2} are set to 0.435 and 0.41 V, respectively. The Q tuning represents an advantage of this design.

Furthermore, in order to validate the inductive behavior of the designed circuit, a study of Differential Active Inductor (DAI) phase characteristics between voltage and current is done. As pictured in Fig. 7, the phase approaches 90° over the entire operating frequency band.

This confirms that the circuit is in its inductive behavior. Note that in the case of exact 90° difference between voltage and current phases, the circuit behaves as an ideal inductor with zero series resistance.[30]

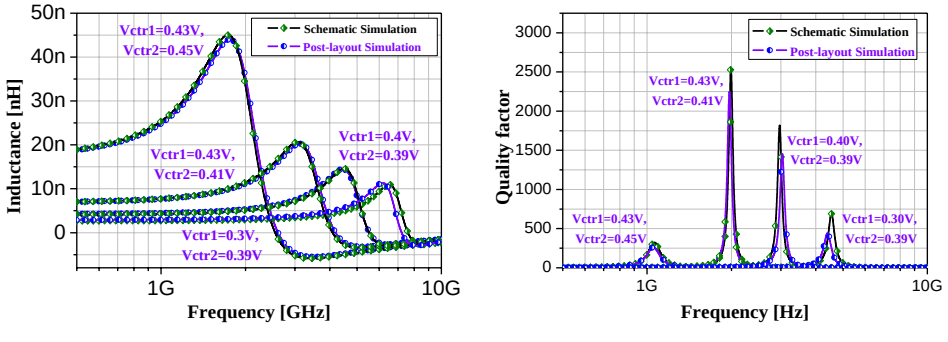

Fig. 6. Comparison between simulation and post-layout simulation of inductance response of the proposed active inductor: (a) inductance response, (b) quality factor response.

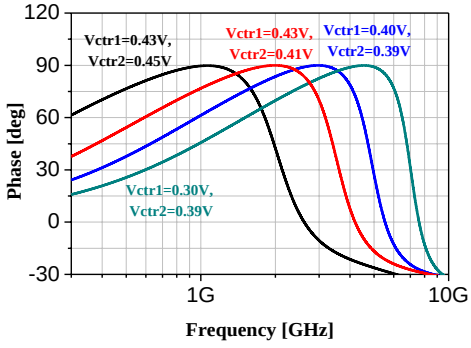

Fig. 7. Post-layout simulation of the impedance phase of the proposed active inductor.

For 1 V supply voltage, the circuit consumes between 0.8 and 1.32 mW for a variation of the inductance value between 44.17 and 10.94 nH, respectively.

Owing to the smallness swing of the inductor control voltages V_{ctr1} and V_{ctr2} and to the bias of all transistors, the circuit of the active inductor will be linear.

Table 2 summarizes the performance of the proposed circuit in order to compare it with other similar works presented in the literature.

Based on this comparative study, it can be noted that this circuit can operate over a wide frequency band with an important adjustment of the inductance value while keeping a high quality factor and low power dissipation. Moreover, this active inductor has a better performance regarding tunability, frequency range, inductance value and quality factor.

The results show that the proposed design techniques are an excellent approach that can be used for example in the design of active tunable filters and Low Noise Amplifiers (LNAs). Particularly, the proposed reconfigurable inductor is suitable for multi-band RF circuits design.

4.2. *Band-pass filter*

The filter was designed to cover the S-band frequencies which range from 2 to 4 GHz. This prototype has been simulated with a nominal bias voltage of 1 V. The input and

Table 2. Comparison of the active inductor performances.

Refs.	Process	V_{dd} (V)	L tuning (nH)	Frequency range (GHz)	Qmax	P_{DC} (mW)
22	90 nm	1.2	0.64–32	0.9–8	134	3.2–19.1
23	0.18 μm	1.8	20–400	0.12–2	560	2.2
22	0.18 μm	1.2	1.7–2.4	1.3–3.2	350	2.2–13
24	0.18 μm	3.3	2–7.5	4.2–4.8	1800	42
25	0.13 μm	1.2	3–5.5	0.83–3.72	N/A	8–13
26	0.13 μm	1.5	0.83–11.7	2.4–3.1	240	22.5
This work	0.13 μm	1	10.94–44.7	1.76–6.55	2,581	0.8–1.32

output buffers are connected to 50 Ω terminators. The results of these simulation measurements are presented below.

4.2.1. *Transmission response*

Through an S-parameter simulation, the frequency response of the BPF ($S21$: forward transmission coefficient, $S11$: input reflection coefficient and $S22$: output reflection coefficient) are, respectively, shown in Figs. 8, 9(a) and 9(b).

The filter is simulated for center frequency of 2 GHz with a transmission coefficient $S21$ of 10.66 dB and a minimum input return loss of −0.88 dB, where the output return loss is around −13.03 dB at 2 GHz. The 3-dB bandwidth is around 620 MHz with power consumption less than 2.38 mW.

The control voltages V_{ctr1}, V_{ctr2} and V_{bias} are fixed, respectively, at 0.51, 0.55 and 0.4 V.

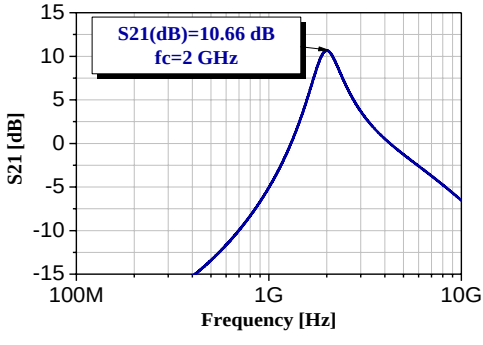

Fig. 8. Simulated BPF transmission coefficient $S21$.

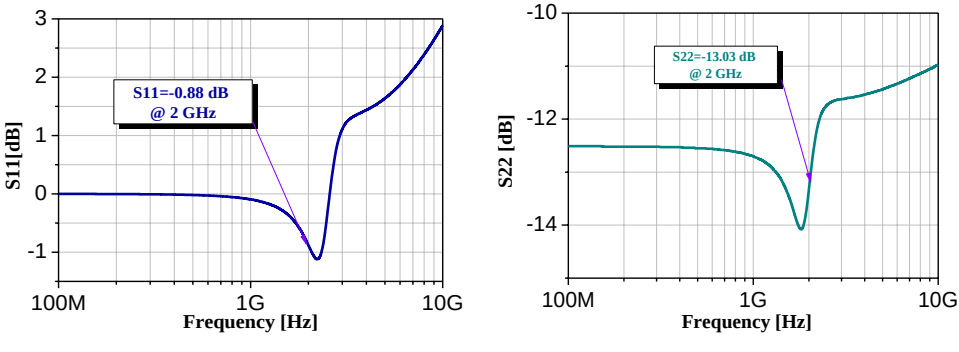

(a) (b)

Fig. 9. Simulated BPF reflection coefficients at a center frequency of approximately 2 GHz: (a) input return loss $S11$, (b) output return loss $S22$.

The S-parameter $S11$ information is often missing in the literature when the performances of active filters are presented; its behavior however is important for the assessment of the stability properties of the circuit.

It is important to remark that the performances in the insertion loss, due to the high Active Inductor (AI) quality factor, are almost similar to a three cell ideal passive filter. Note that this aspect is usually underestimated in the literature and, to our best knowledge, only few works give information about AI stability, power handling and noise.

The next analyses are more focusing on BPF, where the central frequency is 2 GHz.

4.2.2. *Tuning function of the BPF*

Figure 10 shows the simulated frequency characteristics of the filter for various center frequencies. The center frequency tuning can be done through the control DC voltages V_{ctr1} and V_{ctr2}.

Indeed, simulations have been carried out for different combinations of control voltages V_{ctr1} and V_{ctr2} between 0.3 and 0.7 V, in the frequency range from 500 MHz to 10 GHz. This setting causes changing of all parasitic elements of the circuit and subsequently, tuning the active inductor in terms of inductance value, central frequency and quality factor. Tuning of the inductance value provides a variation of the transmission coefficient $S21$ both in center frequency and level. Besides, we can obtain for different combinations of V_{ctr1} and V_{ctr2}, $S21$ responses with the same center frequency but with different level and power consumption.

In order to obtain a filter operating over a wide frequency range, with low power consumption (< 3 mW) and providing approximately a constant gain, only some suitable combinations have been selected. Note that the same phenomenon was found in several studies such as Ref. 29.

The change of the central frequency is obvious. In fact, by analyzing the obtained results, when V_{ctr1} and V_{ctr2} vary, respectively, from 0.39 to 0.51 V and from 0.47 to

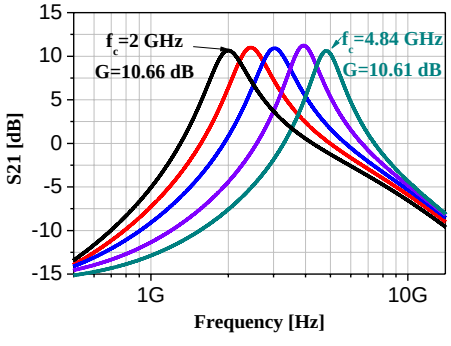

Fig. 10. S21 tuning for different combinations of V_{ctr1} and V_{ctr2}.

Table 3. Different center frequency of BPF with tuning of V_{ctr1} and V_{ctr2}.

V_{ctr1} (mV)	V_{ctr2} (mV)	f_c (GHz)	$S21$ (dB)	P_{DC} (mW)
510	550	2	10.66	2.38
510	520	2.44	10.99	2.56
500	490	3	10.91	2.73
460	470	3.93	11.23	2.84
390	470	4.84	10.61	2.84

0.55 V, it will be possible to control and reconfigure the feedback resistance R_f (implemented by PMOS transistor M_4) from 1.3 to 2.66 kΩ. Therefore, this tuning result causes a variation of current from 257 to 334 μA and a tuning of the center frequency of the BPF from 2 to 4.84 GHz.

Table 3 lists the center frequency, $S21$ parameter and power dissipation values resulting in the tuning of the BPF for different pairs of control voltages V_{ctr1} and V_{ctr2}.

Figure 11 illustrates the behavior of the reflection coefficients $S11$ and $S22$ during the tuning of center frequency of the filter.

It has been found, that the filter has sufficient adaptation to a variety of applications. In fact, the circuit presents a negative input and output return loss for each transmission response (i.e., the five selected combinations). The reflection coefficients $S11$ and $S22$ range, respectively, from −0.88 to −0.97 dB and from −1 3.03 to −16.43 dB over frequency band ranging from 2 to 4.84 GHz.

4.2.3. *Stability analysis*

In order to analyze system stability, the stability factor K_f and the alternative stability factor B_{1f} (or Measure parameter) are simulated. Note that a two-port circuit is unconditionally stable if $K_f > l$ and $B_{1f} > 0$ as given by the following

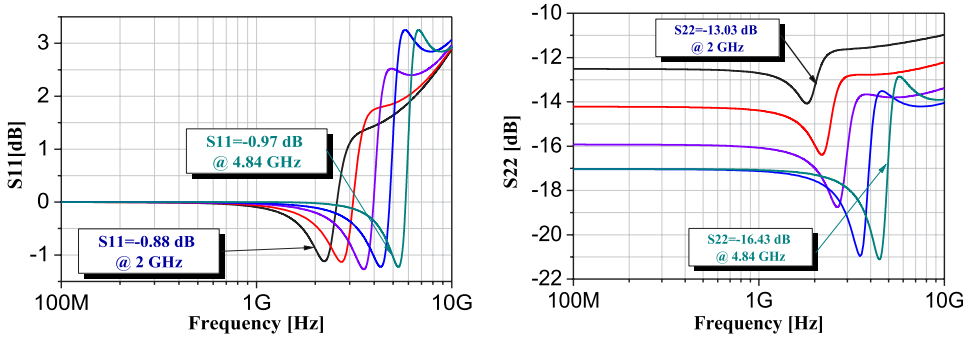

Fig. 11. Simulated BPF reflection coefficients and tuning range capability: (a) Input return loss $S11$ and (b) output return loss $S22$.

expressions[31]:

$$K_f = \frac{1 + |\Delta|^2 - |S_{11}|^2 - |S_{22}|^2}{2|S_{12}||S_{21}|} > 1\,, \tag{12}$$

$$B_{1f} = 1 - |\Delta|^2 + |S_{11}|^2 - |S_{22}|^2 > 0\,, \tag{13}$$

where $\Delta = S_{11}S_{22} - S_{12}S_{21}$.

From the results presented in Fig. 12, we can conclude that the filter is conditionally stable. Nevertheless, a sufficient stability margin is ensured at the operational and higher frequencies since the stability criteria (12) and (13) are simultaneously satisfied for those frequencies.

4.2.4. *Noise figure and linearity*

Because of the presence of active elements (MOSFETs), some noise is brought which has an impact on the response of the filters and could damage the signal of the receiver if there is no amplifying function ahead. For this design, the W- and L-dimensions of transistors in the proposed circuit have been chosen to obtain the lowest noise figure.

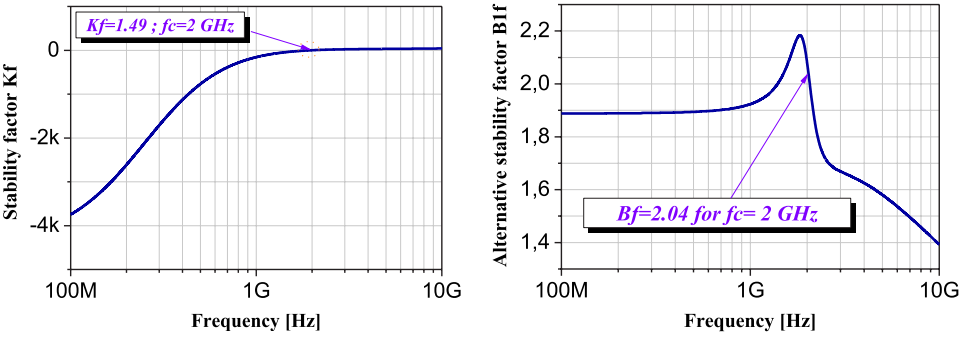

(a) (b)

Fig. 12. Stability properties of BPF: (a) k_f and (b) B_{1f}.

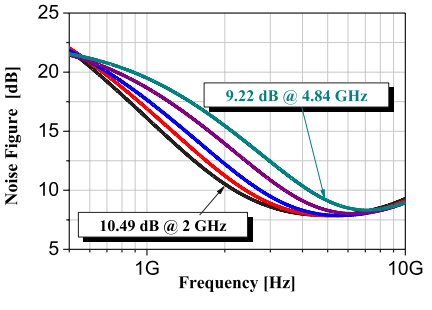

Fig. 13. Noise figure in the multi-band BPF.

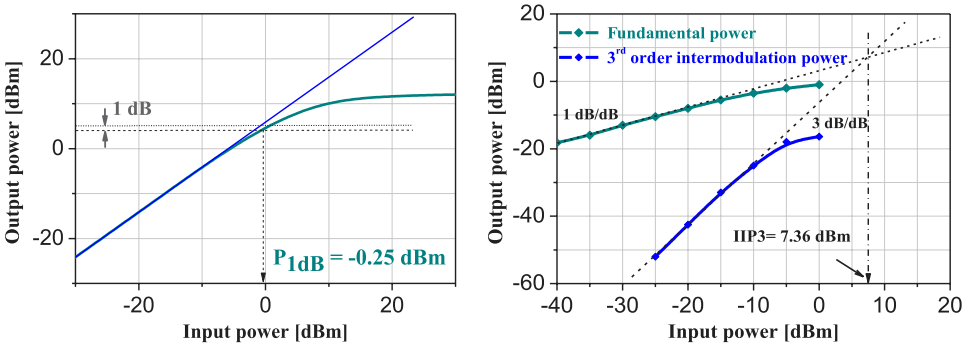

Fig. 14. Linearity of RF BPF: (a) 1 dB compression point and (b) third-order intercept point (IIP3).

The noise figure versus frequency for various control voltages configurations is shown in Fig. 13. The simulated noise figure ranges from 10.49 to 9.22 dB for the entire tuning range 2 to 4.84 GHz.

The linearity of the system is also a very important factor for the evaluation of any circuit. So that, in order to validate this design, the linearity must be assessed. An input referred 1 dB compression point of −0.25 dBm has been obtained as shown in Fig. 14(a).

Furthermore, an inter-modulation simulation is performed by applying two tone signals at 2 and 2.01 GHz to the filter working at 2 GHz in Fig. 14(b). The corresponding IIP3 is approximately 7.36 dBm.

4.2.5. *Post-layout simulation*

For verification, a post-layout simulation of the designed circuit has been performed. Figure 15 shows the acquired post-layout simulation results compared with schematic ones for various center frequencies. We can see that the two curves are then consistent with a light difference, which could be explained by the presence of the parasitic capacitances and resistances. However, we note that these parasites do not affect circuit operation but they generate a deviation.

The comparisons show that schematic simulations for the BPF frequency responses correlate quite well with those of post-layout simulations. The filter has ±4.2% of center frequency error.

4.2.6. *Comparison*

For comparison, the performances of multi-band BPF of other previous research works using active inductor together with this work are summarized in Table 4. Comparison is made on different process technology to have a fair judgment.

Overall, compared with other research works, this multi-band filter has the advantages of compact size with a wide range of center frequencies, which may be

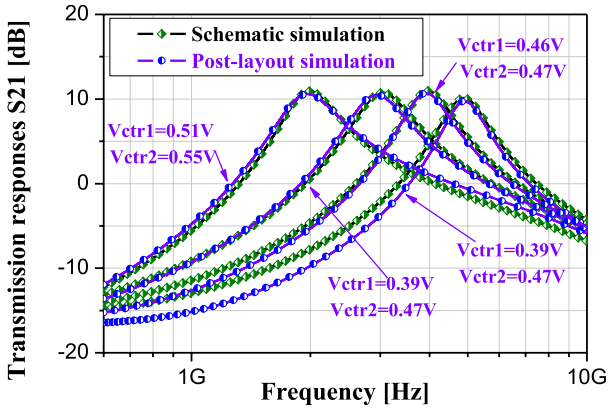

Fig. 15. Comparison between schematic and post-layout simulations of the transmission responses of the multi-band BPF.

Table 4. Comparison of RF BPF performances.

Refs.	Process	V_{dd} (V)	Frequency range (GHz)	$S21$ (dB)	Noise figure (dB)	1-dB (dBm)	IIP3 (dBm)	P_{DC} (mW)
16	0.18 μm	1.8	2.4–12.4	5–23	6–11	N/A	−3.5	2.9
28	0.18 μm	1.8	3.45–3.6	0.2	14.1	N/A	−2.4	28
33	0.18 μm	1.8	0.6–0.9	0.1	11	5	N/A	120
34	0.18 μm	1.8	1.92–3.82	5.99–11.64	18	−15	N/A	28
35	0.13 μm	1.2	0.048–0.78	4.7	24	N/A	3.8	36
36	0.13 μm	1.2	1–2	0.5	19	−21	N/A	30
37	0.13 μm	1.2	1.35–2.53	0.1	N/A	−16	N/A	28.8
This work	0.13 μm	1	2–4.87	10.13–10.95	9.23–10.53	−1.8	7.36	2.38–2.84

suitable and compatible for nano-satellite RF front-end receiver and large number of applications.

However, improved RF BPF or active inductor design for better performance is still possible. In our perspective for this work, as it was presented in several papers such as Ref. 38, we will focus our work to reduce the number of transistors for reducing power consumption and size.

5. Conclusion

In this article, the use of high-Q tunable active inductor in the design of wide tuning RF BPF is presented. The concept is validated thanks to post-layout simulations of designs implemented in 0.13-μm CMOS technology. The main advantage of the proposed multi-band BPF is using the tuning method on the high-Q and low power active inductor instead of a passive inductor in the BPF circuit core.

In the AI circuit, improved tunable quality factor and wide tuning range of resonant frequency are demonstrated. Simulations showed that the AI has an

inductance value tuning range from 10.94 to 44 nH with a maximum quality factor of 2,581 and power consumption less than 1.32 mW. The second-order BPF based on this active inductor shows a tuning range of resonant frequency from 2 to 4.87 GHz providing a voltage gain about 10 dB with less than 10.53 dB noise figure.

References

1. A. Tasic, W. A. Serdijn and J. R. Long, Adaptive multi-standard circuits and systems for wireless communications, *IEEE Circuits Syst. Mag.* **6** (2006) 29–37.
2. T. Soorapanth and S. S. Wong, A 0-dB IL 2140 ± 30 MHz bandpass filter utilizing Q-enhanced spiral inductors in standard CMOS, *IEEE J. Solid-State Circuits* **37** (2002) 579–586.
3. Y. Wu, X. Ding, M. Ismail and H. Olsson, RF bandpass filter design based on CMOS active inductors, *IEEE Trans. Circuits Syst. II, Analog Digit. Signal Process.* **50** (2003) 942–949.
4. T. Bakken and J. Choma, Gyrator-based synthesis of active on-chip inductances, *Analog Integr. Circuits Signal Process.* **34** (2003) 171–181.
5. H. Xiao and R. Schaumann, A 5.4-GHz high-Q tunable active-inductor bandpass filter in standard digital CMOS technology, *Analog Integr. Circuits Signal Process.* **51** (2007) 1–9.
6. G. Leuzzi, V. Stornelli and S. Del Re, A tunable active inductor with high dynamic range for band-pass filter applications, *IEEE Trans. Circuits Syst. II* **58** (2011) 647–651.
7. Y. Wang, L. Ye, H. Liao and R. Huang, Cost-efficient CMOS RF tunable bandpass filter with active inductor-less biquads, *2012 IEEE Int. Symp. Circuits and Systems (ISCAS)*, (Seoul, Korea, 2012), 20–23 May 2012, pp. 2139–2142.
8. H. U. Uyanik and N. Tarim, Compact low voltage high-Q CMOS active inductor suitable for RF applications, *Analog Integr. Circuits Signal Process.* **51** (2007) 191–194.
9. S. V. Krishnamurthy, K. El-Sankary and E. El-Masry, Noise-cancelling CMOS active inductor and its application in RF band-pass filter design, *Int. J. Microw. Sci. Technol.* **2010** (2010) 980957.
10. L. Pantoli, V. Stornelli and G. Leuzzi, Class AB tunable active inductor, *Electron. Lett.* **51** (2015) 65–67, doi: 10.1049/el.2014.3877.
11. H. Schmid, Why the terms 'current mode' and 'voltage mode' neither divide nor qualify circuits, *IEEE ISCAS* (Phoenix-Scottsdale, Arizona, U.S.A., 2002), 26–29 May 2002, pp. II-29–II-32.
12. A. Naderi, A. Khoei, Kh. Hadidi and H. Ghasemzadeh, A new high speed and low power four-quadrant CMOS analog multiplier in current-mode, *AEU-Int. J. Electron. Commun.* **63** (2009) 769–775.
13. A. N. Saatlo and S. Ozoguz, Programmable implementation of diamond-shaped type-2 membership function in CMOS technology, *J. Circuit Syst. Signal Process.* **34** (2014) 321–340.
14. K. S. Hwang, C. S. Cho, J. W. Lee and J. Kim, High quality-factor and inductance of symmetric differential-pair structure active inductor using a feedback resistance design, *2008 IEEE MTT-s International Microwave Symposium; Institute of Electrical and Electronics Engineers*, (Georgia World Congress Center, Atlanta, GA, USA, 2008), 15–20 June 2008, pp. 1059–1062.
15. Q. T. Lai and J. F. Mao, A new floating active inductor using resistive feedback technique, *2010 IEEE MTT-S Int. Microwave Symp. Digest (MTT)*, May 2010, pp. 1748–1751.

16. M. M. Reja, K. Moez and I. Filanovsky, A wide frequency range CMOS active inductor for UWB bandpass filters, *52nd IEEE Int. Midwest Symp. Circuits and Systems, 2009. MWSCAS'09*, (Cancun, Mexico, 2009), 2–5 Aug. 2009, pp. 1055–1058.
17. A. B. Hammadi, M. Mhiri, F. Haddad, S. Saad and K. Besbes, High-Q RF CMOS tunable active inductor for multi-standard applications, *Int. Rev. Model. Simul.* **7** (2014) 567–574.
18. H. H. Hsieh, Y. T. Liao and L. H. Lu, A compact quadrature hybrid MMIC using CMOS active inductors, *IEEE Trans. Microw. Theory Tech.* **55** (2007) 1098–1104.
19. C. E. Saavedra and Y. Zheng, Frequency response comparison of two common active inductors, *Prog. Electromagn. Res. Lett.* **13** (2010) 113–119.
20. A. Thanachayanont, CMOS transistor-only active inductor for IF/RF applications, *IEEE Int. Conf. on Industrial Technology, 2002. IEEE ICIT'02*, Vol. 2, (Shangri-La Hotel, Bangkok, Thailand, 2002), 11–14 Dec. 2002, pp. 1209–1212.
21. A. Thanachayanont and A. Payne, VHF CMOS integrated active inductor, *Electron. Lett.* **32** (1996) 999–1000.
22. C. Hung, K. Cheng, C. Gong, J. Liu, B. Jiang and S. Sun, A 0.9–8 GHz VCO with a differential active inductor for multi-standard wireline SerDes, *IEEE Trans. Circuits Syst. II* **61** (2014) 559–563.
23. J. Xu, C. E. Saavedra and G. Chen, An active inductor-based VCO with wide tuning range and high DC-to-RF power efficiency, *IEEE Trans. Circuits Syst. II* **58** (2011) 462–466.
24. M. A. Abdalla, K. Phang and G. V. Eleftheriades, Printed and integrated CMOS positive/negative refractive-index phase shifters using tunable active inductors, *IEEE Trans. Microw. Theory Tech.* **55** (2007) 1611–1623.
25. H. B. Kia and A. K. A'ain, A wide tuning range voltage controlled oscillator with a high tunable active inductor, *Wirel. Pers. Commun.* **79** (2014) 31–41.
26. Y. J. Jeong, Y. M. Kim, H. J. Chang and T. Y. Yun, Low-power CMOS VCO with a low-current, high-Q active inductor, *IET Microw. Antennas Propag.* **6** (2012) 788–792.
27. A. S. Elwakil and B. J. Maundy, Single transistor active filters: What is possible and what is not, *IEEE Trans. Circuits Syst. I, Regular Papers* **61** (2014) 2517–2524.
28. F. Hu and K. Mouthaan, A high-selectivity active bandpass filter using gyrator based resonators in 0.13-μm CMOS, *2014 IEEE Int. Wireless Symp. (IWS)* (Convention center in X'ian TBD, X'ian, China, 2014), 24 Mar – 26 Mar 2014, pp. 1–4.
29. L. Pantoli, V. Stornelli and G. Leuzzi, Tunable active filters for RF and microwave applications, *J. Circuits Syst. Comput.* **23** (2014) 1450088.
30. L. Pantoli, V. Stornelli and G. Leuzzi, A low-voltage low-power 0.25 μm integrated single transistor active inductor-based filter, *Analog Integr. Circuits Signal Process.* **87** (2016) 463–469.
31. A. Platzker, W. Struble and K. T. Hetzler, Instabilities diagnosis and the role of K in microwave circuits, *IEEE MTT-S Int. Microwave Symp. Digest*, Vol. 3, Atlanta, GA, USA, 1993, pp. 1185–1188.
32. U. L. Rohde and A. K. Poddar, Active inductor oscillator noise dynamics, *2010 IEEE Int. Frequency Control Symp.*, California, USA, 2010, pp. 201–207.
33. J. Manjula and S. Malarvizhi, Performance analysis of active inductor based tunable band pass filter for multiband RF front end, *Int. J. Eng. Technol.* **5** (2013) 2930–2938.
34. K. H. Liang, K. U. O. Chin-Wei and C. H. A. N. Yi-Jen, CMOS RF band-pass filter design using the high quality active inductor, *IEICE Trans. Electron.* **88** (2005) 2372–2376.

35. Z. Gao, J. Ma, M. Yu and Y. Ye, A fully integrated CMOS active bandpass filter for multiband RF front-ends, *IEEE Trans. Circuits Syst. II, Express Briefs* **55** (2008) 718–722.
36. Y. Sun, C. J. Jeong, S. K. Han and S. G. Lee, CMOS on-chip active RF tracking filter for digital TV tuner ICs, *Electron. Lett.* **47** (2011) 407–409.
37. F. Hu and K. Mouthaan, L-band bandpass filter with high out-of-band rejection based on CMOS active series and shunt inductors, *IEEE MTT-S Int. Microwave Symp. (IMS2014)*, Tampa Bay, Florida, 2014, pp. 1–3.
38. P. Branchi, L. Pantoli, V. Stornelli and G. Leuzzi, RF and microwave high-Q floating active inductor design and implementation, *Int. J. Circuit Theory Appl.* **43** (2015) 1095–1104.